Lead chloride perovskites for *p*-type transparent conductors: A critical theoretical reevaluation

Sanlue Hu,1 Bing Xia,1 Yanfa Yan,2,* and Zewen Xiao1,*

¹Wuhan National Laboratory for Optoelectronics, Huazhong University of Science and Technology, Wuhan 430074, China

²Department of Physics and Astronomy and Wright Center for Photovoltaics Innovation and Commercialization, The University of Toledo, Toledo, Ohio 43606, United States

*Emails: <u>yanfa.yan@utoledo.edu</u> (Y.Y.); <u>zwxiao@hust.edu.cn</u> (Z.X.)

Abstract:

Recently, lead chloride perovskites represented by CsPbCl₃ have been theoretically predicted to be ideal *p*-type transparent conductors and hence attracted a lot of attention. However, experimentally, these materials have long been known to be insulators that can hardly be converted to *p*-type conductors by extrinsic doping. In this work, we systematically evaluate the *p*-type dopability of lead chloride perovskites by density functional theory calculations. We find that the previously predicted dopability is due to an overestimation caused by the functionals employed that gives an unreasonable high-lying valence band maximum. The hybrid functional with an optimized mixing parameter and the inclusion of spin–orbit coupling gives suitable description of the band edge positions and thus a better assessment of the dopability. Our defect calculations suggest that lead chloride perovskites are intrinsically insulating and can hardly be converted to *p*-type conductors due to the lack of effective dopants, in agreement with the experimental observations. Our results highlight the importance of the suitable description of band edge positions on the prediction of defect properties and dopability of semiconductors.

I. INTRODUCTION

Transparent conductors (TCs) play important roles in optoelectronic devices [1–3]. Currently, most of the commercial TCs are based on n-type oxides, often referred as to transparent conductive oxides (TCOs) [4–7], whereas the realization of their stable p-type counterparts is difficult [8–10]. The challenge in achieving p-type TCOs is attributed to the deep and localized valence band maximums (VBMs) consisting of O 2p orbitals [11], which impedes the generation and transport of holes. Therefore, raising and delocalizing the VBM, e.g., by employing cations with high-lying quasi-closed d^{10} or s^2 orbitals (e.g., d^{10} or s^2) that can hybridize with O 2p orbitals, has been the common strategy to design p-type TCs [12,13]. Over the past two decades, many p-type TCs, represented by a series of Cu(I)-based compounds such as CuAlO₂ [14,15], have been discovered. However, their performances are still insufficient for commercial applications.

On the other hand, over the past decade, lead halide perovskites have been widely studied for optoelectronic applications such as solar cells [16,17], light-emitting diodes [18,19], and photodetectors [20,21]. The superior optoelectronic properties of lead halide perovskites are partially attributed to the strong anti-bonding coupling between the quasi-closed Pb 6s² and the halogen p orbitals, which leads to small hole masses and shallow cation vacancies [22–25]. From a materials design perspective, it is of particular interest to see if such a s–p anti-bonding coupling in wide-bandgap lead halide perovskites can raise the VBM higher enough to enable good *p*-type conductivity, like the case of CuAlO₂. Zhang et al. [26] have recently proposed wide-bandgap lead chloride perovskites represented by CsPbCl₃ as potential ideal *p*-type TCs based on density functional theory (DFT) calculations. Their defect calculations indicate that these compounds can be easily doped heavily *p*-type at the Pb-poor condition, which has attracted a lot of attention.

The dopability of a semiconductor depends on multiple factors [27], among which the band edge positions play a dominant role and have been the most important descriptor. Generally, the lower the conduction band minimum (CBM), the easier the *n*-type doping. On the other hand, the higher the VBM, the simpler the *p*-type doping. Empirically, for oxide semiconductors, the CBM threshold for *n*-type doping and the VBM threshold for *p*-type doping consistently lie at about –4 and –6eV, respectively, with respect to the vacuum level [13].

As shown in Fig. 1, the typical *n*-type TCOs such as ZnO, SnO₂, In₂O₃, and amorphous In–Ga–Zn–O (IGZO), have CBM positions below –4 eV, while the typical *p*-type TCOs such as CuAlO₂, CuGaO₂, SrCu₂O₂, and NiO, exhibit VBMs above –6 eV [13,28]. For lead chloride perovskites, experimental studies [29–32] have shown that the CBMs are relatively high while the VBMs are comparatively deep, implying both *n*- and *p*-type doping difficulties. Experimentally, the lead chloride perovskites have long been known to be insulators [33–36], and no successful *p*-type conductivity via doping routes [37,38]. The contradiction between the experimental observations and Zhang et al.' theoretical predictions motivated us to carefully reevaluate the dopability of these lead chloride perovskites.

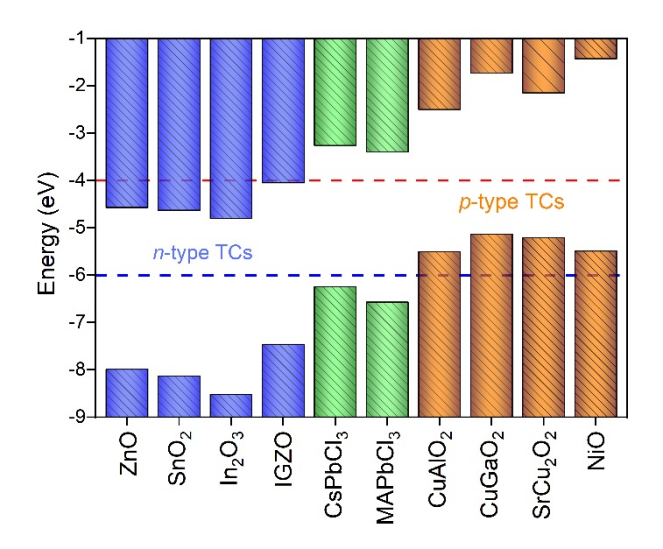


FIG. 1. Band alignment of lead chloride perovskites along with typical n- and p-type transparent conductors. The red and blue dash lines mark the empirical threshold values for n- and p-type doping in TCOs, respectively.

In this work, taking CsPbCl₃ as an example, we systematically reevaluate the dopability of lead chloride perovskites by DFT calculations. We show that the hybrid functional with the optimized mixing parameters and the inclusion of spin—orbit coupling provides reasonable predictions of band edge positions and is thus suitable to assess the dopability. Our defect calculations suggest that lead chloride perovskites are intrinsically insulating and can hardly be doped to be good *p*-type conductors by the considered dopants including Cu, Ag, Na, K and Rb. Our results contradict the previous prediction but are in good agreement with the experimental

observations.

II. COMPUTATIONAL METHOD

DFT calculations were conducted using the projection-augmented wave (PAW) method as implemented in the Vienna Ab initio Simulation Package (VASP) [39]. The plane-wave cutoff energy was set to 350 eV. The semilocal Perdew-Burke-Ernzerhof (PBE) [40] generalized-gradient approximation (GGA) functional was used for all structural relaxations. Γ -centered k-meshes with k-spacing of 0.2 Å⁻¹ and the Γ -only k-mesh were used for primitive cells and the 160-atoms supercell for modeling defects, respectively. The structures were fully relaxed until the force on each atom was <0.01 eV/Å. For the room temperature orthorhombic CsPbCl₃ (space group *Pnma*), the GGA functional gave a bandgap of 2.54 eV, which is slightly smaller than the experimental value of 2.97 eV [35]. When the spin-orbit coupling (SOC) that is important for correctly describing the electronic structure was included, the calculated bandgap was significantly reduced to 1.52 eV. The Heyd-Scuseria-Ernzerhof (HSE) [41,42] hybrid functional with the standard mixing parameter of 25% and the neglect of SOC provided an overestimated bandgap of 3.32 eV. When SOC was included, the calculated bandgap reduced to 2.28 eV, which is still much smaller than the experimental value. With the mixing parameter increased to 45%, the calculated bandgaps with and without SOC were increased to 3.99 and 2.95 eV, respectively. For all calculations expect for structural relaxations, we have employed all the above 6 functionals, hereafter denoted as GGA, GGA+SOC, $HSE^{\alpha=0.25}$, $HSE^{\alpha=0.25}$ +SOC, $HSE^{\alpha=0.45}$, and $HSE^{\alpha=0.45}+SOC$, respectively. Phase diagrams of the Cs-Pb-Cl system were drawn by the Chesta code [43] with the calculated total energies of all known phases in the Inorganic Crystal Structure Data (ICSD), including Cs₄PbCl₆ and CsPb₂Cl₅, which were not considered in Ref. [26] (see Table S1 in the Supplemental Material [44]).

For a defect (D) in a charge state q, the formation enthalpy ($\Delta H_{\mathrm{D},q}$) was calculated through the equation [45,46]:

$$\Delta H_{D,q} = E_{D,q} - E_{h} + q(E_{V} + E_{F}) + \sum n_{i}\mu_{i} + E_{corr}$$
 (1)

where $E_{D,q}$ and E_h are the total energies of the supercell with the defect (D) in the charge q and the perfect host supercell, respectively. E_F is the Fermi level referred to VBM level (E_V). n_i

indicates the number of i atom added (n_i <0) or removed (n_i >0) when a defect is formed, and μ_i is the chemical potential of the i atom which can be expressed with respect to that of an element phase (μ_i^{el}) by $\mu_i = \mu_i^{\text{el}} + \Delta \mu_i$, where the $\Delta \mu_i$ is constrained in the chemical potential window. E_{corr} is the total correction for the defect formation enthalpy, including the band-filling correction, the potential alignment correction, and the image charge correction [45–48].

The charge transition level $\varepsilon(q/q')$ was calculated by using the equation:

$$\varepsilon(q/q') = \frac{\Delta H_{\mathrm{D},q'} - \Delta H_{\mathrm{D},q}}{q - q'} \tag{2}$$

where $E_{D,q}(E_{D,q'})$ is the total energy of a defect at the charge state q(q').

The defect density was calculated by the statistic equation [49,50]:

$$c_{D,q}(E_{F,\mu},T_{D}) = N_{D,q} \exp\left[\frac{-\Delta H_{D,q}(E_{F,e},\mu)}{k_{B}T_{D}}\right]$$
(3)

where $E_{F,e}$ is the equilibrium E_F , $N_{D,q}$ is the density of possible sites for defects, k_B is Boltzmann constant, and T_D is the temperature where defects are formed. The defects formed at T_D are assumed to be frozen at the room temperature. Herein, 300 K is taken for the room temperature solution process. The $E_{F,e}$ was determined by solving the following semiconductor statistic equations self-consistently so as to satisfy the charge neutrality condition [49,50].

$$\sum_{i} \sum_{j} q_{i} c_{D_{j}, q_{i}} - N_{e} + N_{h} = 0$$
 (4)

$$N_{\rm e} = N_{\rm c} \exp\left[\frac{-(E_{\rm F,e} - E_{\rm g})}{k_{\rm B}T_{\rm M}}\right]$$
 (5)

$$N_{\rm h} = N_{\rm v} \exp\left[\frac{-E_{\rm F,e}}{k_{\rm B}T_{\rm M}}\right] \tag{6}$$

$$N_{\rm c} = 2 \frac{\left(2\pi m_{\rm e}^* k_{\rm B} T_{\rm M}\right)^{3/2}}{h^3} \tag{7}$$

$$N_{\rm v} = 2 \frac{\left(2\pi m_{\rm h}^* k_{\rm B} T_{\rm M}\right)^{3/2}}{h^3} \tag{8}$$

where N_e and N_h are densities of the electron and hole, respectively; N_c and N_v are effective densities of states in the conduction band and valence band, respectively; m_e^* and m_h^* are the

effective masses of electrons and holes, respectively; $E_{\rm g}$ is the calculated bandgap; $T_{\rm M}$ is the temperature for measuring electrical properties (herein $T_{\rm M}=300$ K for room-temperature measurements). The calculated $E_{\rm g}$, $m_{\rm e}^*$, $m_{\rm h}^*$, $N_{\rm e}$ and $N_{\rm h}$ with different functionals are summarized in Table S2 in the Supplement Material [44]. Based on the HSE $^{\alpha=0.45}+$ SOC calculations, we revaluated the doping properties of Cu, Ag, Na, K and Rb. It should be emphasized that to more correctly determine the upper limits of the dopant chemical potentials, all possible dopant-containing phases must be considered as the competing secondary phases. We considered *all* Rb-, K-, Na-, Ag- and Cu-containing phases that are available in the ICSD database. For a given ($\Delta\mu_{\rm Cs}$, $\Delta\mu_{\rm Pb}$, $\Delta\mu_{\rm Cl}$) in the chemical window of CsPbCl₃, the upper limits of the dopant chemical potentials are determined by the following inequations, with the results summarized in Table S3.

$$\Delta\mu_{\rm Rb} < \Delta H \,(\rm Rb) = 0 \,\, \rm eV \tag{9}$$

$$\Delta\mu_{\rm Rb} + \Delta\mu_{\rm Cl} < \Delta H \,(\rm RbCl) = -4.28 \,\, \rm eV \tag{10}$$

$$\Delta\mu_{Rb} + \Delta\mu_{Pb} < \Delta H (RbPb) = -0.66 \text{ eV}$$
 (11)

$$3\Delta\mu_{Cs} + \Delta\mu_{Rb} + 5\Delta\mu_{Cl} < \Delta H (Cs_3RbCl_5) = -16.55 \text{ eV}$$
 (12)

$$2\Delta\mu_{\rm Cs} + \Delta\mu_{\rm Rb} + 6\Delta\mu_{\rm Cl} < \Delta H (K_2 \text{RbCl}_6) = -12.62 \text{ eV}$$
 (13)

$$\Delta\mu_{K} < \Delta H(K) = 0 \text{ eV}$$
 (14)

$$\Delta\mu_{K} + \Delta\mu_{Cl} < \Delta H (KCl) = -4.31 \text{ eV}$$
 (15)

$$2\Delta\mu_{K} + \Delta\mu_{Pb} + 6\Delta\mu_{Cl} < \Delta H (K_2 PbCl_6) = -12.45 \text{ eV}$$
 (16)

$$\Delta\mu_{K} + 2\Delta\mu_{Pb} + 5\Delta\mu_{Cl} < \Delta H \text{ (KPb}_{2}Cl_{5}) = -11.57 \text{ eV}$$
 (17)

$$\Delta\mu_{\text{Na}} < \Delta H \,(\text{Na}) = 0 \text{ eV} \tag{18}$$

$$\Delta\mu_{\text{Na}} + \Delta\mu_{\text{Cl}} < \Delta H \text{ (NaCl)} = -4.02 \text{ eV}$$
 (19)

$$\Delta \mu_{Ag} < \Delta H (Ag) = 0 \text{ eV}$$
 (20)

$$\Delta\mu_{Ag} + \Delta\mu_{Cl} < \Delta H \text{ (AgCl)} = -1.44 \text{ eV}$$
 (21)

$$\Delta\mu_{Cs} + \Delta\mu_{Ag} + 3\Delta\mu_{Cl} < \Delta H (CsAgCl_3) = -5.58 \text{ eV}$$
 (22)

$$2\Delta\mu_{C_{S}} + \Delta\mu_{A_{G}} + 3\Delta\mu_{C_{I}} < \Delta H (Cs_{2}AgCl_{3}) = -10.27 \text{ eV}$$
 (23)

$$\Delta\mu_{\rm Cs} + \Delta\mu_{\rm Ag} + 2\Delta\mu_{\rm Cl} < \Delta H \,({\rm KAgCl_2}) = -5.87 \,\,{\rm eV}$$
 (24)

$$\Delta\mu_{Cu} < \Delta H (Cu) = 0 \text{ eV}$$
 (25)

$$\Delta\mu_{C_1} + 2\Delta\mu_{C_1} < \Delta H \text{ (CuCl}_2) = -0.60 \text{ eV}$$
 (26)

$$\Delta\mu_{Cs} + 2\Delta\mu_{Cl} + 3\Delta\mu_{Cl} < \Delta H (CsCu_2Cl_3) = -4.15 \text{ eV}$$
 (27)

$$\Delta\mu_{\rm Cs}^{+} + \Delta\mu_{\rm Cu}^{+} + 3\Delta\mu_{\rm Cl}^{-} < \Delta H \,(\rm CsCuCl_3) = -4.97 \,\,\rm eV$$
 (28)

$$2\Delta\mu_{C_{S}} + \Delta\mu_{C_{I}} + 4\Delta\mu_{C_{I}} < \Delta H (Cs_{2}CuCl_{4}) = -9.54 \text{ eV}$$
 (29)

$$3\Delta\mu_{Cs} + 2\Delta\mu_{Cu} + 5\Delta\mu_{Cl} < \Delta H (Cs_3Cu_2Cl_5) = -12.88 \text{ eV}$$
 (30)

III. RESULTS AND DISCUSSION

The defect formation enthalpies and thus the dopability of a semiconductor depends strongly on the chemical potential. Therefore, it is important to figure out the correct chemical potential window. We confirmed that the phase diagrams calculated with different functionals are almost the same (see Fig. S1 in Ref. [44]). For instance, the one calculated with $HSE^{\alpha=0.45}+SOC$ is taken for discussion, as shown in Fig. 2. The chemical potential boundary of $CsPbCl_3$ is determined from its phase equilibrium with the Cs_4PbCl_6 , $CsPb_2Cl_5$, Cs_2PbCl_6 and elemental Pb, respectively [51]. The lines AB and CD represent the Pb-rich and Pb-poor conditions, respectively. Points A and D indicate the Cl-poor (Pb-rich and Cs-rich) and Cl-rich (Pb-poor and Cs-poor) conditions, respectively. Obviously, if Cs_4PbCl_6 and $CsPb_2Cl_5$ are artificially neglected, the chemical window of $CsPbCl_3$ along with the $\Delta\mu_{Cl}$ and $\Delta\mu_{Cs}$ ranges will be overestimated (see Figs. S2 and S3), which will then leads to overestimated dopability of $CsPbCl_3$, as will be discussed later.

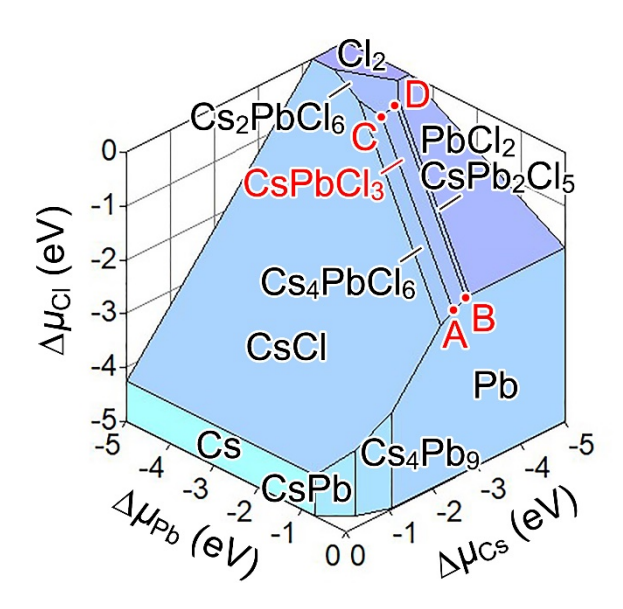


FIG. 2. HSE^{α=0.45}+SOC calculated chemical window of CsPbCl₃.

The formation enthalpies (ΔH) of intrinsic defects in CsPbCl₃ under different potential points were calculated with various functionals and shown in Figs. S4-S6 [44]. The calculated maximum and minimum $E_{\rm F,e}$ values, denoted as $E_{\rm F,e}^{\rm max}$ and $E_{\rm F,e}^{\rm min}$, are obtained at points A and D, respectively. Fig. 3 summarizes the $E_{\rm F,e}^{\rm max}$ and $E_{\rm F,e}^{\rm min}$ along with the relative band edge positions aligned by referring the common average potentials [52]. The GGA functional without SOC predicts a bandgap of 2.54 eV and unipolar p-type conduction. Interestingly, the $E_{\rm Fe}^{\rm min}$ is even below the VBM, which indicates that CsPbCl₃ can be doped degenerated p-type under the Pb-poor condition. When SOC is included, the CBM position is lowered by 0.98 eV due to the SOC-induced splitting of Pb 6p states, while the VBM position is almost unchanged. As a result, the GGA+SOC results seem to indicate that CsPbCl₃ can exhibit bipolar conduction ranging from degenerated p-type to moderate n-type. However, these GGA and GGA+SOC results contradict the experimental results. The contradiction originates from the unreasonable bandgap and band edge positions, which are caused by the self-interaction error associated with the semilocal GGA. The self-interaction can be partially corrected by the hybrid functionals. The standard $HSE^{\alpha=0.25}$ provides a bandgap of 3.32 eV, with the VBM downshifted by 0.51 eV and the CBM upshifted by 0.27 eV as compared with those calculated by GGA. The predicted conduction is still unipolar p-type, but the $E_{\rm F,e}^{\rm min}$ raises to 0.13 eV above the VBM, with a high hole density (N_h) of 3.2×10¹⁷ cm⁻³. With the Cs₄PbCl₆ and CsPb₂Cl₅ phases being artificially excluded, the $E_{\rm F,e}^{\rm min}$ is reduced to 0.11 eV and the $N_{\rm h}$ is overestimated to 6.4×10¹⁷ cm⁻³ accordingly (see Fig. S7 in Ref. [44]). These results almost reproduce the results in Ref. [26] in which the SOC was neglected. With the SOC included, the bandgap is reduced to 2.28 eV by the CBM lowering. The $E_{\rm Fe}^{\rm min}$ is upshifted to 0.20 eV and the $N_{\rm h}$ is reduced to 3.2×10¹⁷ cm⁻³ accordingly. To further correct the bandgap and band edges, the mixing parameter should be optimized to a larger value. We found that the HSE $^{\alpha=0.45}$ +SOC provides a bandgap of 2.95 eV, fairly close to the experimental bandgap value of 2.97 eV. The resulted VBM is 0.90 eV lower than that of GGA and 0.39 eV lower than that of HSE $^{\alpha=0.25}$. The $E_{\rm Fe}^{\rm min}$ is 0.44 eV above the VBM, which yields a low N_h of 1.1×10^{11} cm⁻³ that can hardly be measured by a Hall effect equipment (cf. $N_h = 1.3 \times 10^{17} \text{ cm}^{-3}$ for CuAlO₂ [14]). The HSE $^{\alpha=0.45}$ +SOC results suggest that even if synthesized under the Pb-poor condition, CsPbCl₃ is electrically insulating. These results contradict the previous prediction but agree well with the experimental results so far. As the $HSE^{\alpha=0.45}+SOC$ simultaneously corrects the errors associated with self-interaction and SOC, it can provide a reasonably good prediction of the absolute band edge positions, as supported by the slab model calculations (see Figs. S8). Therefore, it is reasonable to believe that $HSE^{\alpha=0.45}+SOC$ provides better insights than the other five methods.

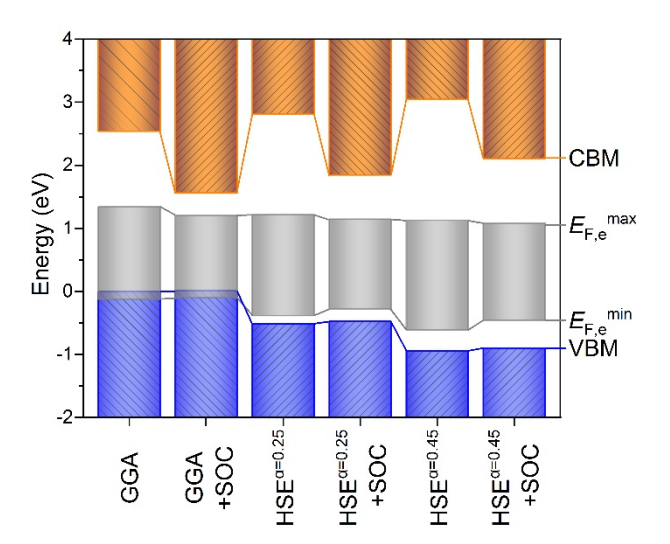


FIG. 3. The calculated maximum and minimum $E_{F,e}$ values ($E_{F,e}^{max}$ and $E_{F,e}^{min}$, respectively) along with the CBM and VBM positions with different functionals. The CBMs and VBMs are aligned by referring the common average potentials. The zero energy is set to the GGA-VBM.

Finally, we consider if the intrinsically insulating CsPbCl₃ can be converted to p-type TC

by extrinsic doping. Based on the "doping limit rule" proposed by Zunger et al., [53–57] the dopability of a semiconductor can be theoretically evaluated by the dopant pinning energy $(E_{pin,p})$ and $E_{pin,n}$ for p-type and n-type doping, respectively), where if a dopant would move the E_F to this level, then compensating vacancies will be spontaneously created at no cost. If equilibrium holds, it will be impossible to shift the $E_{\rm F}$ beyond the $E_{\rm pin}$. Practical doping will only occur if the $E_{pin,p}$ or $E_{pin,n}$ lie in the valence or conduction band, respectively, and not in the bandgap. For CsPbCl₃, under the Pb-poor condition, the $E_{pin,p}$ is minimum and lies at 0.56 eV below the VBM (Fig. 4a). This indicates that CsPbCl₃ can be doped p-type if there is a suitable dopant. Herein, Rb⁺, K⁺, Na⁺, Ag⁺, and Cu⁺ were chosen as dopant candidates, as they have ionic radii comparable to that of Pb²⁺. For each dopant, we considered three possible doping sites (i.e., the Pb-site, the interstitial site and Cs-site), the ΔH of which were calculated with the HSE $^{\alpha=0.45}$ +SOC method. The results (see Figs. S9 and S10 in Ref. [43]) show that the Pb-site is the most energetically favored site for these dopants. Rb-on-Pb (Rb_{Pb}), K-on-Pb (K_{Pb}), Na-on-Pb (Na_{Pb}), and Ag-on-Pb (Ag_{Pb}) substitutions are all shallow acceptors (see Figs. 4b-4e), which result from the shallow nature of the V_{Pb} and the relatively high ionicity of the dopants. For Rb_{Pb}, Na_{Pb}, and Ag_{Pb}, the minimum ΔH are achieved at point D, a Pb-poor condition. However, their ΔH values are larger than that of the intrinsic V_{Cs} , which indicates that the Rb, Na and Ag dopants can hardly improve the N_h . For K_{Pb} , the lowest ΔH is obtained at point C, a Pb-poor condition too. The ΔH of K_{Pb} is slightly lower than that of the intrinsic V_{Cs} (Fig. 4c). As a result, the formation of K_{Pb} acceptors can push the $E_{F,e}$ slightly down to 0.33 eV above the VBM and increase the N_h slightly to 1.1×10^{13} cm⁻³, which, however, is several orders of magnitude lower than those of the typical p-type TCOs (cf. $N_h = 1.3 \times 10^{17} \text{ cm}^{-3}$ for CuAlO₂ [14]). For the Cu dopant, Cu-on-Pb substitution (Cu_{Pb}) is a deep acceptor with the (0/+1) transition located at 0.59 eV above the VBM (Fig. 4f), indicating that in the p-type region, Cupb is neutral and does not contribute to p-type conductivity. The deep nature of Cu_{Pb} can be understood from the facts that there exist many 6-coordinated Cu(II)-based halides such as $ACuCl_3$ (A = Cs, Rb, K) [58–60] and $Cs_4CuSb_2Cl_{12}$ [61,62] and that monovalent Cu(I) is unstable within 6-coordinated halogen octahedra [63]. On the other hand, the undesired formation of Cu interstitial (Cu_i) donors can partially compensate the holes created by the

intrinsic acceptors and decrease the conductivity. These results indicate that it would be difficult to convert CsPbCl₃ to a p-type conductor with high N_h even by extrinsic doping using Rb, K, Na, Ag, and Cu dopants, which explains the difficulty of extrinsic p-type doping in CsPbCl₃.

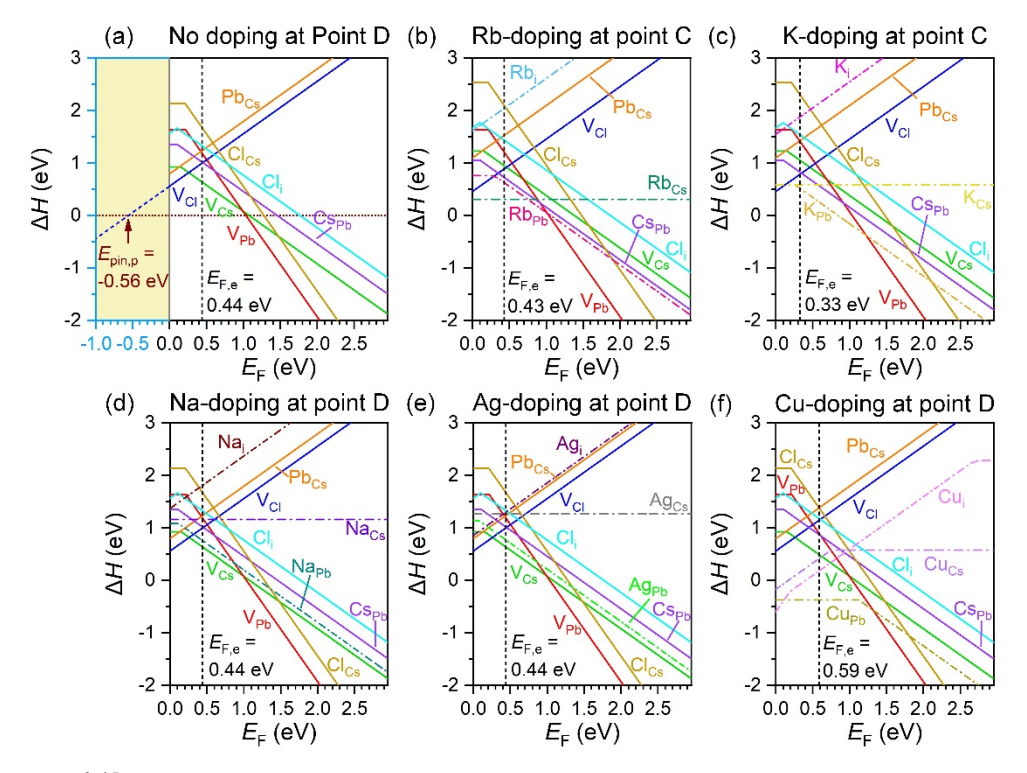


FIG. 4. HSE $^{\alpha=0.45}$ +SOC-calculated formation enthalpies (ΔH) of defects in CsPbCl₃ under Pb-poor conditions (i.e., points C or D in Fig. 2): (a) No doping; (b) Rb-doping; (c) K-doping; (d) Na-doping; (e) Ag-doping; and (f) Cu-doping. The calculated equilibrium $E_F(E_{F,e})$ are indicated by vertical black dash lines.

VI. CONCLUSION

In summary, we have examined the *p*-type dopability of lead chloride perovskites by various functionals. We found that the semilocal functionals give overestimated high-lying VBMs due to the well-known self-interaction error, leading to overestimated *p*-type dopability. Hybrid functionals, with optimized mixing parameter and the inclusion of SOC, provide suitable prediction of the band edge positions and thus better evaluation of the dopability. Our defect calculations indicate that lead chloride perovskites are intrinsically insulating and can hardly be converted to *p*-type conductors by extrinsic doping using Rb, K, Na, Ag, and Cu dopants. Our results agree well with the experimental results and highlight the importance of

band edge positions on the prediction of defect properties and dopability.

ACKNOWLEDGMENTS

This work was financially supported by the National Natural Science Foundation of China (NSFC) (Grant No. 51972130), the Thousand Young Talents Program of China, the Startup Fund of Huazhong University of Science and Technology, and the Director Fund of Wuhan National Laboratory for Optoelectronics. The work at The University of Toledo was supported by National Science Foundation under contract no. DMR–1807818.

REFERENCES

- [1] K. L. Chopra, S. Major, and D. K. Pandya, Thin Solid Films **102**, 1 (1983).
- [2] C. G. Granqvist, Sol. Energy Mater. Sol. Cells **91**, 1529 (2007).
- [3] S. Calnan and A. N. Tiwari, Thin Solid Films **518**, 1839 (2010).
- [4] H. Ohta, K. Nomura, H. Hiramatsu, K. Ueda, T. Kamiya, M. Hirano, and H. Hosono, Solid. State. Electron. 47, 2261 (2003).
- [5] K. Nomura, H. Ohta, A. Takagi, T. Kamiya, M. Hirano, and H. Hosono, Nature **432**, 488 (2004).
- [6] K. Nomura, A. Takagi, T. Kamiya, H. Ohta, M. Hirano, and H. Hosono, Japanese J. Appl. Physics, Part 1 Regul. Pap. Short Notes Rev. Pap. 45, 4303 (2006).
- [7] H. Hosono, Thin Solid Films **515**, 6000 (2007).
- [8] M. Joseph, H. Tabata, and T. Kawai, Japanese J. Appl. Physics, Part 2 Lett. **38**, L1205 (1999).
- [9] D. S. Ginley and J. D. Perkins, in *Handbook Transparent Conduct*. (Springer US, Boston, MA, 2011), pp. 1–25.
- [10] K. H. L. Zhang, K. Xi, M. G. Blamire, and R. G. Egdell, J. Phys. Condens. Matter 28, 383002 (2016).
- [11] J. Robertson and S. J. Clark, Phys. Rev. B Condens. Matter Mater. Phys. 83, 075205 (2011).
- [12] H. Kawazoe, H. Yanagi, K. Ueda, and H. Hosono, MRS Bull. 25, 28 (2000).
- [13] H. Hosono, Jpn. J. Appl. Phys. **52**, 090001 (2013).

- [14] H. Kawazoe, M. Yasukawa, H. Hyodo, M. Kurita, H. Yanagi, and H. Hosono, Nature **389**, 939 (1997).
- [15] H. Yanagi, S. I. Inoue, K. Ueda, H. Kawazoe, H. Hosono, and N. Hamada, J. Appl. Phys.88, 4159 (2000).
- [16] A. Kojima, K. Teshima, Y. Shirai, and T. Miyasaka, J. Am. Chem. Soc. **131**, 6050 (2009).
- [17] M. M. Lee, J. Teuscher, T. Miyasaka, T. N. Murakami, and H. J. Snaith, Science (80-.). **338**, 643 (2012).
- [18] Z. K. Tan, R. S. Moghaddam, M. L. Lai, P. Docampo, R. Higler, F. Deschler, M. Price, A. Sadhanala, L. M. Pazos, D. Credgington, F. Hanusch, T. Bein, H. J. Snaith, and R. H. Friend, Nat. Nanotechnol. 9, 687 (2014).
- [19] H. Cho, S. H. Jeong, M. H. Park, Y. H. Kim, C. Wolf, C. L. Lee, J. H. Heo, A. Sadhanala, N. S. Myoung, S. Yoo, S. H. Im, R. H. Friend, and T. W. Lee, Science (80-.). 350, 1222 (2015).
- [20] L. Dou, Y. M. Yang, J. You, Z. Hong, W. H. Chang, G. Li, and Y. Yang, Nat. Commun.5, 5404 (2014).
- [21] H. Wei, Y. Fang, P. Mulligan, W. Chuirazzi, H. H. Fang, C. Wang, B. R. Ecker, Y. Gao,M. A. Loi, L. Cao, and J. Huang, Nat. Photonics 10, 333 (2016).
- [22] W. J. Yin, T. Shi, and Y. Yan, Appl. Phys. Lett. **104**, 063903 (2014).
- [23] W. J. Yin, T. Shi, and Y. Yan, Adv. Mater. 26, 4653 (2014).
- [24] Z. Xiao and Y. Yan, Adv. Energy Mater. 7, 1701136 (2017).
- [25] Z. Xiao, Z. Song, and Y. Yan, Adv. Mater. **31**, 1803792 (2019).
- [26] P. Zhang, S. Yu, X. Zhang, and S. H. Wei, Phys. Rev. Mater. 3, 055201 (2019).
- [27] A. Goyal, P. Gorai, S. Anand, E. S. Toberer, G. J. Snyder, and V. Stevanović, Chem. Mater. 32, 4467 (2020).
- [28] J. Robertson and B. Falabretti, in *Handbook Transparent Conduct*. (Springer US, Boston, MA, 2011), pp. 27–50.
- [29] R. Comin, G. Walters, E. S. Thibau, O. Voznyy, Z. H. Lu, and E. H. Sargent, J. Mater. Chem. C 3, 8839 (2015).
- [30] V. K. Ravi, G. B. Markad, and A. Nag, ACS Energy Lett. 1, 665 (2016).
- [31] C. Li, J. Wei, M. Sato, H. Koike, Z. Z. Xie, Y. Q. Li, K. Kanai, S. Kera, N. Ueno, and J.

- X. Tang, ACS Appl. Mater. Interfaces 8, 11526 (2016).
- [32] S. Tao, I. Schmidt, G. Brocks, J. Jiang, I. Tranca, K. Meerholz, and S. Olthof, Nat. Commun. 10, (2019).
- [33] O. Busmundrud and J. Feder, Solid State Commun. 9, 1575 (1971).
- [34] Z. Liu, J. A. Peters, C. C. Stoumpos, M. Sebastian, B. W. Wessels, J. Im, A. J. Freeman, and M. G. Kanatzidis, in *Hard X-Ray, Gamma-Ray, Neutron Detect. Phys. XV*, edited by M. Fiederle, A. Burger, L. Franks, and R. B. James (2013), p. 88520A.
- [35] M. Sebastian, J. A. Peters, C. C. Stoumpos, J. Im, S. S. Kostina, Z. Liu, M. G. Kanatzidis, A. J. Freeman, and B. W. Wessels, Phys. Rev. B - Condens. Matter Mater. Phys. 92, 235210 (2015).
- [36] S. Jiang, X. Wang, Y. Wu, Y. W. Li, Q. Zhang, G. W. Li, Y. Wu, W. Zhang, X. Zhang,B. Wang, J. Chen, and W. Lei, Mater. Lett. 236, 26 (2019).
- [37] K. Watanabe, M. Koshimizu, T. Yanagida, Y. Fujimoto, and K. Asai, Jpn. J. Appl. Phys. 55, 02BC20 (2016).
- [38] R. Zhang, Y. Yuan, J. Li, Z. Qin, Q. Zhang, B. Xiong, Z. Wang, F. Chen, X. Du, and W. Yang, J. Lumin. **221**, 117044 (2020).
- [39] G. Kresse and J. Furthmüller, Phys. Rev. B Condens. Matter Mater. Phys. **54**, 11169 (1996).
- [40] J. P. Perdew, K. Burke, and M. Ernzerhof, Phys. Rev. Lett. 77, 3865 (1996).
- [41] J. Heyd, G. E. Scuseria, and M. Ernzerhof, J. Chem. Phys. 118, 8207 (2003).
- [42] J. Paier, M. Marsman, K. Hummer, G. Kresse, I. C. Gerber, and J. G. Angyán, J. Chem. Phys. 124, 154709 (2006).
- [43] N. Hatada, Chesta Software for Creating Chemical Potential Diagrams. https://www.aqua.mtl.kyoto-u.ac.jp/wordpress/chestaEng.html (accessed: May 24th, 2020).
- [44] See the Supplemental Material at http://*** for slab models; all known phases for diffrent phase diagrams; calculated bandgaps, effective masses and effective densities of states in the conduction band and valence band with different functionals; calculated phase diagrams; defect formation enthalpies for intrinsic and extrinsic defect calculations.
- [45] C. G. Van de Walle and J. Neugebauer, J. Appl. Phys. 95, 3851 (2004).

- [46] S. Lany and A. Zunger, Phys. Rev. B Condens. Matter Mater. Phys. **78**, 235104 (2008).
- [47] C. Freysoldt, J. Neugebauer, and C. G. Van De Walle, Phys. Rev. Lett. **102**, 016402 (2009).
- [48] Y. Kumagai and F. Oba, Phys. Rev. B Condens. Matter Mater. Phys. **89**, 195205 (2014).
- [49] J. Ma, S. H. Wei, T. A. Gessert, and K. K. Chin, Phys. Rev. B Condens. Matter Mater. Phys. 83, 245207 (2011).
- [50] J. H. Yang, W. J. Yin, J. S. Park, J. Ma, and S. H. Wei, Semicond. Sci. Technol. 31, 083002 (2016).
- [51] L. B. Matyushkin and V. A. Moshnikov, Semiconductors **51**, 1337 (2017).
- [52] M. H. Du, J Phys Chem Lett **6**, 1461 (2015).
- [53] F. Zhang, S. H. Wei, and A. Zunger, Phys. Rev. Lett. 84, 1232 (2000).
- [54] S. B. Zhang, S. H. Wei, and A. Zunger, Phys. Rev. B Condens. Matter Mater. Phys. 63, 1 (2001).
- [55] C. H. Park, S. B. Zhang, and S. H. Wei, Phys. Rev. B Condens. Matter Mater. Phys. **66**, 1 (2002).
- [56] S. B. Zhang, J. Phys. Condens. Matter 14, (2002).
- [57] A. Zunger, Appl. Phys. Lett. **83**, 57 (2003).
- [58] C. J. Kroese, W. J. A. Maaskant, and G. C. Verschoor, Acta Crystallogr. Sect. B Struct. Crystallogr. Cryst. Chem. **30**, 1053 (1974).
- [59] W. J. Crama, J. Solid State Chem. **39**, 168 (1981).
- [60] H. Zhou, X. Liu, G. He, L. Fan, S. Shi, J. Wei, W. Xu, C. Yuan, N. Chai, B. Chen, Y. Zhang, X. Zhang, J. Zhao, X. Wei, J. Yin, and D. Tian, ACS Omega 3, 14021 (2018).
- [61] B. Vargas, E. Ramos, E. Pérez-Gutiérrez, J. C. Alonso, and D. Solis-Ibarra, J. Am. Chem. Soc. 139, 9116 (2017).
- [62] T. Cai, W. Shi, S. Hwang, K. Kobbekaduwa, Y. Nagaoka, H. Yang, K. Hills-Kimball, H. Zhu, J. Wang, Z. Wang, Y. Liu, D. Su, J. Gao, and O. Chen, J. Am. Chem. Soc. 142, 11927 (2020).
- [63] Z. Xiao, K. Z. Du, W. Meng, D. B. Mitzi, and Y. Yan, Angew. Chemie Int. Ed. 56, 12107 (2017).